AGU ADVANCING EARTH AND SPACE SCIENCE

Geophysical Research Letters®

RESEARCH LETTER
10.1029/2021GL096156

Parker Ice Tongue Collapse, Antarctica, Triggered by Loss of Stabilizing Land-Fast Sea Ice

Rodrigo Gomez-Fell[1], Wolfgang Rack[1], Heather Purdie[2], and Oliver Marsh[3]

[1]Gateway Antarctica, School of Earth and Environment, University of Canterbury, Christchurch, New Zealand, [2]School of Earth and Environment, University of Canterbury, Christchurch, New Zealand, [3]British Antarctic Survey, Cambridge, UK

Key Points:

- The 2020 Parker Ice Tongue collapse was a result of repeated total fast-ice break-out and very likely unprecedented in at least 169 years
- Periods of continuous ice tongue growth coincided with extended periods of land-fast sea ice coverage
- The seasonal variability of ice tongue dynamics is linked to the stabilizing effect of land-fast sea ice buttressing

Supporting Information:

Supporting Information may be found in the online version of this article.

Correspondence to:

R. Gomez-Fell,
rodrigo.gomezfell@pg.canterbury.ac.nz

Citation:

Gomez-Fell, R., Rack, W., Purdie, H., & Marsh, O. (2022). Parker Ice Tongue collapse, Antarctica, triggered by loss of stabilizing land-fast sea ice. *Geophysical Research Letters*, *49*, e2021GL096156. https://doi.org/10.1029/2021GL096156

Received 14 SEP 2021
Accepted 30 NOV 2021

Author Contributions:

Conceptualization: Rodrigo Gomez-Fell
Formal analysis: Rodrigo Gomez-Fell
Investigation: Rodrigo Gomez-Fell
Methodology: Rodrigo Gomez-Fell
Supervision: Wolfgang Rack, Heather Purdie, Oliver Marsh
Writing – original draft: Rodrigo Gomez-Fell
Writing – review & editing: Rodrigo Gomez-Fell, Wolfgang Rack, Heather Purdie, Oliver Marsh

Abstract After a likely multi-century period of intermittent calving, the full length of Parker Ice Tongue (18 km or 41 km^2), calved in March 2020 co-incident with repeated summer break-outs of the surrounding land-fast sea ice. A complete ice tongue collapse for these otherwise stable glaciological landmarks along the Victoria Land Coast is previously unrecorded. Prior to break-off, we found an inverse correlation between fast ice extent and ice tongue velocities ($R = -0.62$; $R^2 = 0.39$). The short summer period, characterized by decreased land-fast sea ice extent, showed around 11% higher velocities compared to winter. Any previous events of comparable magnitude could not have occurred since at least ~1,850, assuming continuous growth (~193m yr^{-1}) derived from the last 60 years of satellite observations. We highlight the vulnerability of the ice tongue once left exposed to oceanic processes, which poses questions about the fate of other ice tongues if land-fast sea ice decreases more broadly in the future.

Plain Language Summary Ice tongues are iconic glaciological landmarks along the Victoria Land Coast in the western Ross Sea of Antarctica. Forming at the seaward margin of marine-terminating glaciers, they extend many kilometers from the coast out to the sea. Over much of the year, ice tongues are embedded and protected by land-fast sea ice (fast-ice), which is sea ice attached to land. Fast-ice recession can trigger ice tongue calving, which is an indicator of environmental change. We document a unique event in observational history, which is the complete loss of Parker Ice Tongue after exceptional seasons of repeated and complete fast-ice break-out. An event of this magnitude could have only occurred previously around the 1850s or more likely much longer back in time. We show that ice tongue integrity, evolution, and motion are affected by fast ice variability. Using satellite image time series, we observed that fast-ice delayed Parker Ice Tongue collapse by protecting it from oceanic processes like currents and waves. It demonstrates the importance of coastal sea ice for these floating ice masses. It also confronts us with the question about the fate of such ice tongues if coastal sea ice coverage decreases as a result of future climate change.

1. Introduction

The Antarctic ice sheet discharges its mass through outlet glaciers and ice streams forming downstream of the grounding line either (to a larger part) ice shelves or (to a smaller part) ice tongues. These floating ice masses occupy 74% of the total Antarctic coastline (Bindschadler et al., 2011). Ice shelves are an important regulator of grounded ice discharge exerting a buttressing force that affects the ice flow dynamics in the interior of the ice sheet (Depoorter et al., 2013; Pritchard et al., 2012; Rack & Rott, 2004; Rignot et al., 2019; Rott et al., 2018). Ice tongues, unconstrained at their lateral margins, are typically fed by one marine terminating glacier, and often embedded in land-fast sea ice (hereafter fast-ice). Exposure to atmospheric and oceanographic forcing and less protection to their sides makes them vulnerable to changing climatic conditions, and a sentinel for local environmental change (Truffer & Motyka, 2016). Here we report the complete break-off of the Parker Ice Tongue at the Borchgrevink Coast as an early sign of such a change.

Ice tongues are a distinctive feature of the Victoria Land Coast in the Western Ross Sea. This section of the Antarctic coast has 32 outlet glaciers that end as ice tongues (Fountain et al., 2017). A decrease in area for some ice tongues and ice shelves between 1960–1963 and 1972–1973 and an increase afterward was documented (Frezzotti, 1993), but overall relatively stable frontal position in the last 60 years have been observed (Fountain et al., 2017; Frezzotti, 1993; Miles et al., 2013). Different reasons have been given to explain the relative stability of outlet glaciers and ice tongues in the Western Ross Sea, such as cooler air temperatures (Miles et al., 2013), the formation of marine ice at the base (Frezzotti, 1997), and a cold coastal ocean current (Stevens et al., 2017).

Fluctuations of these and other related variables, such as the abundance of fast ice, could alter the boundary conditions which control the mass balance and length of ice tongues. We examine one of these variables, namely fast-ice extent, and its influence and stabilizing effect on the Parker Ice Tongue (PIT) prior to its collapse in 2020.

Sea ice is an important driver of change for coastal Antarctic land ice (Baumhoer et al., 2021; Massom et al., 2018), and fast-ice has a significant role in various ice-ocean related processes. Fast-ice has been associated with polynya formation (Brett et al., 2020; Fraser et al., 2019; Mezgec et al., 2017; Nihashi & Ohshima, 2015), ice shelf disintegration/stability (Massom et al., 2018), Ice Shelf Water formation (Haas et al., 2021), and ice tongue calving events (Robinson & Haskell, 1990; Stevens et al., 2013). Fast-ice has been observed to protect ice tongues and when absent calving events are more likely to occur (Massom, 2003; Robinson & Haskell, 1990; Stevens et al., 2013). It has been suggested that the existence of fast-ice is essential for ice tongue growth (Wearing et al., 2020). Massom et al. (2010) observed multiyear fast-ice mechanically coupled with the Mertz ice tongue and proposed that fast-ice can have an important role in the stabilization of ice sheet maritime margins. Information about fast-ice stabilization of ice shelves or ice tongues is scarce (Massom et al., 2010; Robinson & Haskell, 1990) and few studies exists on the seasonal relationship between ice shelf dynamics and sea ice (Greene et al., 2018; Zhou et al., 2014). The effect of ice melange, a consolidated agglomeration of icebergs and fast-ice, on glacier margins has been studied more broadly for Greenland. Ice melange is strongly correlated with glacier retreat and advance (Howat et al., 2010; Moon et al., 2015), can alter the buttressing effect of ice tongues affecting marine terminating glacier dynamics (Krug et al., 2015; Todd & Christoffersen, 2014), and can stabilize the ice margin impeding calving (Amundson et al., 2010; Cassotto et al., 2021; Robel, 2017).

Oceanic processes also have an effect on ice tongue stability affecting its mechanics and dynamics. Tidal currents can exert considerable lateral force over glacier tongues, creating lateral flexure and controlling along flow velocities which affect its dynamics (Legrésy et al., 2004). Holdsworth (1982) showed that the curvature of the Erebus Ice Tongue is a result of the ocean current pressure and in a two-way interaction ice tongues also affect local oceanographic dynamics (Stevens et al., 2014, 2017). Tides generate vertical displacement of ice tongues due to tide wave oscillation (Holdsworth, 1969; Padman et al., 2018). Holdsworth and Glynn (1978) found that stresses induced by tides are higher at the grounding line but at the same time that the grounding line is not a common point of failure of ice tongues.

The objective of this paper is twofold; first we describe the PIT 2020 break-up, and second we analyze the stabilizing properties of fast-ice and its relation with ice tongue dynamics. We show evidence of fast-ice mechanical stabilization of the ice tongue, delaying its break-up, and seasonal changes in ice dynamics associated with oscillations in fast-ice extent. Our observations are remote sensing based, mostly from Sentinel-1 SAR images. We also use optical and historical aerial photography to better constrain the length history of PIT.

2. PIT and the Ice Tongues Along the Borchgrevink Coast

Out of the 32 Victoria Land Coast ice tongues, 19 are found along the Borchgrevink Coast. The most prominent ice tongues in this area are Aviator, Mariner, Borchgrevink and Tucker (Frezzotti, 1997). PIT is located at Lady Newnes bay at 165.833 E and 73.857 S (Figure 1a). Compared to some of its neighbors the PIT has a smaller size and catchment. For example, the Aviator Ice Tongue, Mariner Ice Tongue and the massive Drygalski Ice Tongue are all wider and longer, with grounded catchments basins larger than 7,000 km^2 (Frezzotti, 1997). Based on the analysis of the Antarctic REMA DEM, Parker glacier has a catchment of 188 km^2. The length of the PIT has varied between 16 to 21 km in the last 60 years (Figure 2). Its width varies from 1.3 km at the tip to 2.4 km near the grounding line. In relation to other Western Ross Sea ice tongues, the PIT is long and narrow with its tip bending slightly northwards. We attribute the bending to the asymmetric grounding line velocities, which are slightly higher in the South.

3. Data and Methods

3.1. Surface Velocities From Sentinel-1

Ice surface velocities were derived from 93 pairs Sentinel-1 12-day repeat pass of synthetic aperture radar (SAR) images in Single Look Complex (SLC) format. Data were acquired in interferometric wide-swath (IW) mode and delivered with a pixel spacing of 2.3 m in slant range and 14.1 m in azimuth. The image time series used

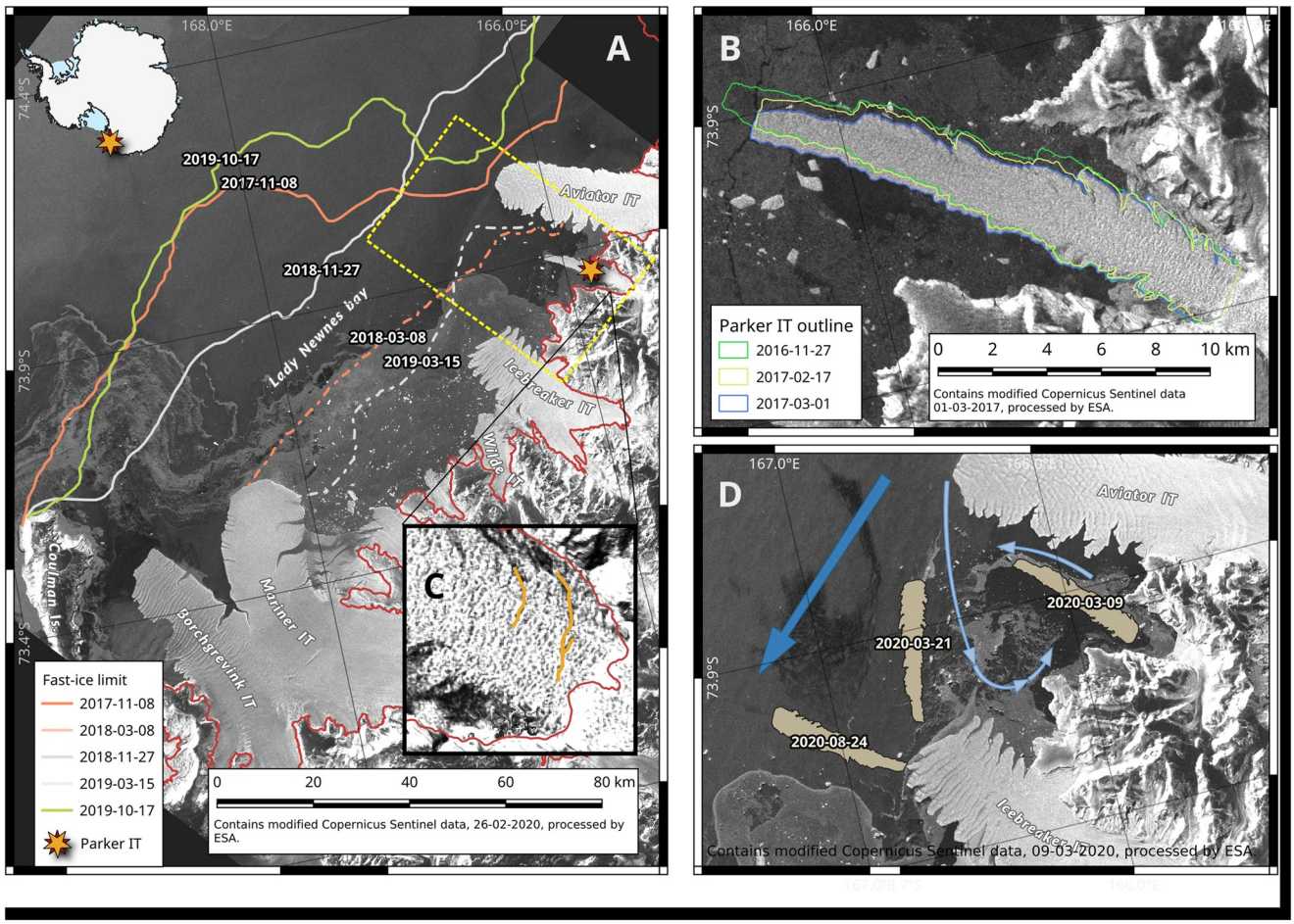

Figure 1. Sentinel-1 synthetic aperture radar image sequence of the southern Borchgrevink coast acquired during complete fast-ice break-outs plotted with (a) spring maximum (solid lines) and autumn minimum (dashed lines) extent of fast-ice between November 2017 and October 2019 (2017–2018: orange, 2018–2019: light gray, 2019: green). The box (yellow dashed line) delimits the area used for detailed fast-ice analysis. The ASAID grounding line (Bindschadler et al., 2011) is also shown (red); (b) northward ice tongue shift during the 2017 fast ice break-out; (c) rift formation in the grounding zone during the 2017 fast-ice break-out; (d) drift of PIT after break-off in 2020, showing the main south-north coastal current (blue) and the possible circulation pattern around PIT (light blue). All images in Antarctic polar-stereographic projection EPSG:3031.

for ice surface velocity calculations spans from the 5 February 2017 to the 26 February 2020 acquired in exactly the same imaging geometry. We use a SAR intensity tracking algorithm to obtain the ice tongue surface velocities (Strozzi et al., 2002; Wegmüller et al., 2016). The small baseline of Sentinel-1 orbits allows for a very accurate sub-pixel co-registration of the image (Wegmüller et al., 2016). The intensity tracking algorithm uses a cross-correlation method over image patches of two previously co-registered images to estimate offsets from the SAR speckle pattern (Strozzi et al., 2002). To estimate the errors of the tracking algorithm we followed Vijay and Braun (2017). Our error estimate for more than 89% of the pairs is < 0.215 m d^{-1} or 78.4 m yr^{-1} (for details see supplements).

3.2. Semi-Automatic Determination of Land-Fast Sea Ice Area Extent

For the satellite based detection of the fast-ice boundary we make use of the fact that pack ice is very dynamic whereas fast-ice being attached to land remains stagnant. Following a semi-automatic approach similar to the one described by Mahoney and Eicken (2004) and Li et al. (2018) we identify fast-ice from areas with similar radar intensity levels in pairs of consecutive co-registered Sentinel-1 images. Rapid changes in surface properties of fast-ice (e.g., by melting) can significantly alter the radar backscattering, creating errors when comparing two consecutive acquisitions. We found that Sentinel-1 12 days repeat pass images normally show sufficiently small change. Because we use exact repeat pass images with identical imaging geometry we can neglect variations in

radar backscattering which arise from changing radar incidence angles. Image differences are post-processed using the following steps; a gaussian filter with a sigma value of five, an edge detection filter, automatic thresholding to produce a binary result, and finally, the application of a morphology filter. After a visual inspection 5% of the results needed fine-tuning, mainly due to our algorithm underestimating fast-ice area. Our final product at 100 m pixel resolution was compared between February-2017 to February-2018 with a pan-continental fast-ice data set at lower resolution (1 km) (Fraser et al., 2020). We also did a visual comparison of our results with MODIS optical data when possible; both data sets showed good agreement with our analysis.

From our fast-ice area product, we get a maximum and minimum fast-ice extent for each year and the total area in square kilometers for each pair of images. To compare fast-ice area changes with ice tongue dynamics, we defined a rectangular region of fast-ice influence around the PIT. This region satisfies the following conditions: (a) a good representation of the seasonal fast-ice coverage of the larger area, and (b) encompassing the embayment between the adjacent ice tongues. We found that a polygon with 3 times the length of PIT corresponds well to these requirements. It results in a maximum fast-ice area of 1,150 km^2 around the ice tongue which has a size of about 50 km^2 (Figure 1a).

3.3. PIT Length

We use aerial photographs and satellite imagery to digitally map the PIT outline from 1957 to 2020 (Table S4 in Supporting Information S1). The 1957, 1962 and 1963 aerial photographs were acquired by the U.S. Geological Survey (USGS) and the 1980 image is a declassified satellite image from the Key Hole (KH-9) mission (Burnett, 2012). We geo-referenced the USGS aerial photos and the declassified satellite images using a GIS software manually selecting tie points with a Sentinel-2 optical image from 2016. The position derived from the 1962 Trigonometron aerial photo is likely slightly overestimated, as it had to be referenced to the overlapping PIT area of the 1963 USGS image due to the lack of GCP points on land. Our estimation of the 1957 ice tongue frontal position is based on the 1962–1980 growth rate because of missing tie points to the 1962 or 1963 USGS images. For 1973 and from 1988 onwards we used a series of different optical and radar satellite images from the Landsat (ETM, OLI), Sentinel-1 and -2 missions. This allowed us to estimate the frontal position of PIT over a period of 63 years prior to break-off (Figure 2).

The length of the PIT was measured from the grounding line (Bindschadler et al., 2011) to the frontal position following the central flow-line. For the last 20 years of the time series we selected a yearly satellite image from the month of November, unless a sizable calving event occurred. The frontal advance rate of each period was calculated dividing the length difference by the amount of days between images. The accuracy of the length measurement depends on the pixel resolution of the sensor and for the USGS aerial photographs and KH-9 image also on the quality of our geo-referencing. The latter was assessed by comparison to known independent ground control points which were not used for geo-referencing. For these images the error estimates are below 200 m, and for all images the errors are smaller than the symbol size on Figure 2.

4. PIT Dynamic Behavior and Fast-Ice Influence Prior to Break-Up

The complete break-off of PIT (41 km^2) near the grounding line and over its full length (18 km) occurred between 26 February and 4 March 2020. The calving of the entire ice tongue, and in fact complete calving of any Antarctic ice tongue, has not been observed before. Based on the growth rates (Figure 2) we infer that for PIT an event of that scale has likely not occurred over at least 169 years. PIT dynamics appear to follow closely the seasonal fast-ice extent oscillation, and the surrounding fast-ice is most likely an important driver in its structural stability and for the longevity of the ice tongue.

4.1. PIT Growth Rate

We established five main periods of continuous growth between calving events (Figure 2): 1963 to 1980 (187m yr^{-1}), 1988 to 2005 (160m yr^{-1}), 2005 to 2008 (201m yr^{-1}), 2011 to 2016 (223m yr^{-1}) and 2017 to 2020 (236m yr^{-1}). The mean growth rate of the PIT prior to its break-off for the last 20 years disregarding any major calving is 197.9 ± 59.3 m yr^{-1}, and for the whole observation period 193.1 ± 57.4 m yr^{-1}. Considering the

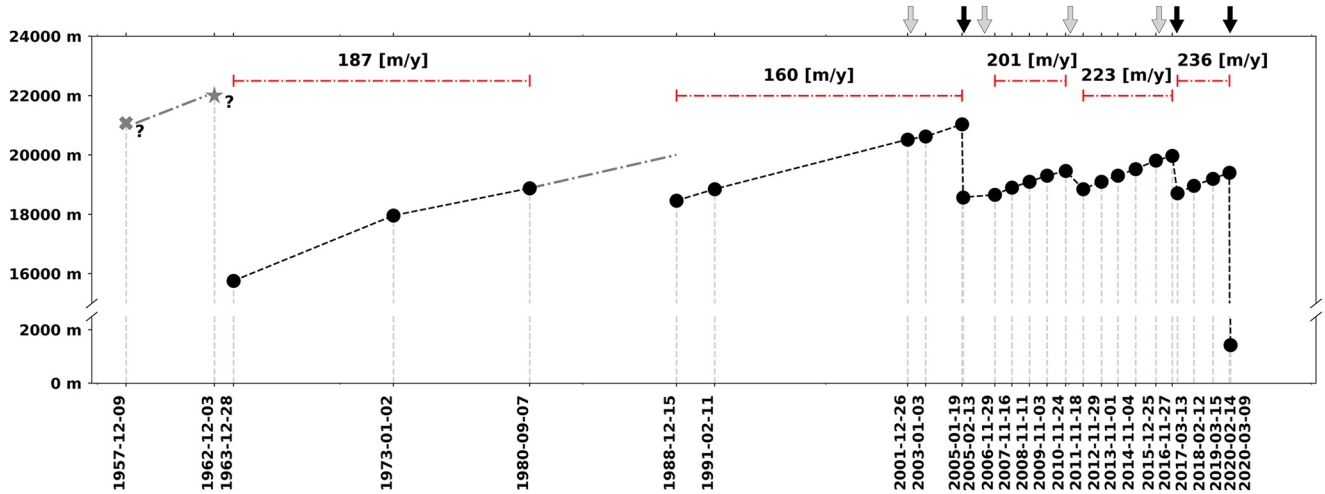

Figure 2. PIT length for the period 1957 to 2020 measured from the grounding line to the tip along the center flow line. The black dashed lines connect positions with net growth. The star symbol marks the estimated length in 1962 (see text) and the x symbol marks the estimated length in 1957 (see text). The gray dash-dot line indicates the possible growth path of the ice tongue. The red dash-dot lines indicate long periods of continuous growth between calving events with the corresponding growth rate between first and last image of the period (28-12-1963 to 07-09-1980, 15-12-1988 to 19-01-2005, 13-02-2005 to 11-11-2008, 03-09-2011 to 27-11-2016 and 13-03-2017 to 02-14-2020). Annual average net growth rates for periods longer than 2 years are shown. Arrows indicate short (<1 month; gray) and long (>1 month; black) periods of fast ice break out since 2001. The 1957, 1962 and 1963 lengths were obtained from the 1963 U.S. Geological aerial photographic Survey mission and the 1980 position from declassified KH-9 mission data. All other lengths are obtained from either Landsat (1973, 2001 to 2014), Sentinel-1 (2017–2020), or Sentinel-2 (2016) satellite images.

1963–2020 growth rate it would take 108.8 ± 24.9 years of continuous growth to re-advance to the maximum observed length (~21 km).

Over the last 15 years, three periods of continuous growth with rates similar to the mean surface ice velocity correspond well with periods of persistent fast-ice extent (see supplement). Fast-ice holds the ice tongue flanks, maintaining its integrity, preventing calving and promoting growth, similar to melange (Amundson et al., 2010; Krug et al., 2015; Todd et al., 2019). This can be noticed for the calving event in 2005 when an iceberg of ~3.22 km^2 detached from the ice tongue tip. The iceberg broke at the same point where the minimum fast-ice extent was observed for that year, suggesting that calving is controlled by the variability of fast-ice extent and how this in return influences ice tongue growth.

Prior to the ice tongue collapse, we can identify four major calving events, which are defined as losing at least 2000 m in length (Figure 2). They happened in early 1963 (Frezzotti, 1997), between October 1980 and December 1988, in 2005, and in 2017. We can relate major calving events after 2000 to periods of low fast-ice coverage from Fraser et al. (2020) and from this study.

4.2. Fast-Ice Coverage in the Proximity of PIT (2017–2020)

According to the Fraser et al. (2020) data set (2000–2017) and our own observations (2017–2020), complete break up of fast-ice in the vicinity of PIT has occurred seven times in the last two decades (2002, 2005, 2006, 2011, 2016, 2017 and 2020). It is not possible to determine the exact duration of fast-ice free conditions due to the restricted temporal resolution of the fast-ice product. But we observed that 2005, similar to 2017 and 2020, had a longer fast-ice free period. For the calving events in 2005 and 2017, and for all the growth periods that overlap these dates, the growth rate is either negative (major calving) or below 100m yr^{-1} (minor calving). Over the last 20 years of observations, 2004/05, 2016/17 and 2019/20 were exceptional fast-ice seasons with a long duration of low fast-ice coverage. On the other hand, over extended periods without break-out multi-year fast ice persisted in some areas for as long as four years.

During the 2017–2020 period the area around PIT was mostly covered in fast-ice. The largest but short-lived fast-ice extent was observed in October 2019. Winter 2018 had a maximum extent lower than the 2019 maximum for the whole embayment (Figure 1), but it persisted much longer at the full extent from end of May 2018 into the next year to January 2019. During the low extent periods from February to mid-March 2018 and from beginning

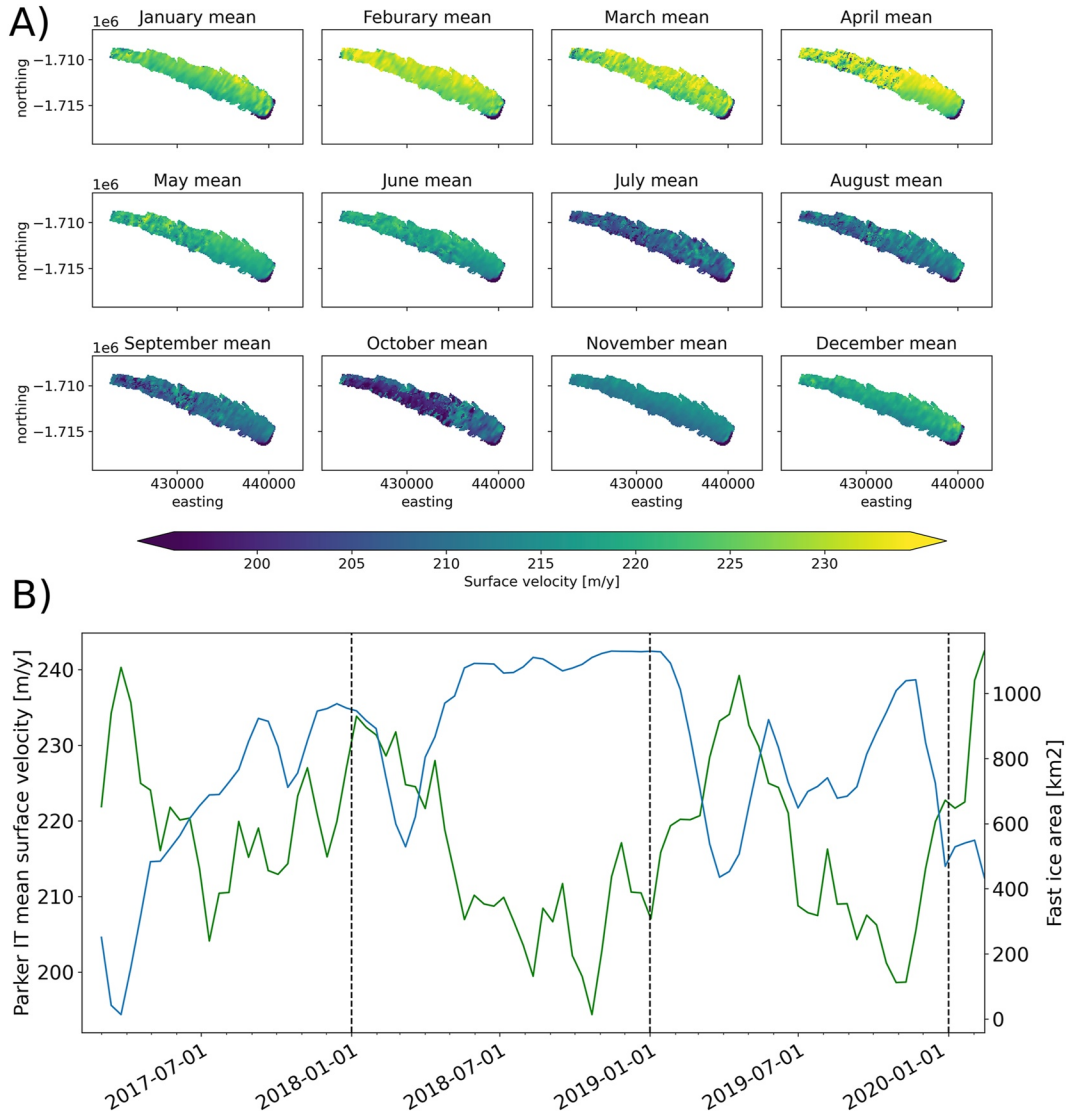

Figure 3. (a) Monthly average ice velocity fields of Parker Ice Tongue (PIT) derived from Sentinel-1 SAR offset tracking between February 2017 to February 2020. (b) Fast-ice area surrounding PIT (blue) based on yellow rectangle in Figure 1 plotted with mean surface velocity (green line).

of March to the end of May 2019 (Figure 3b) the ice tongue was still completely (2018) or almost completely (2019) surrounded by fast-ice.

The area of fast-ice assumed to be of influence for the PIT ice mechanics and dynamics is highlighted in yellow in Figure 1a and the fast-ice coverage in this box is plotted in Figure 3b for the 2017–2020 period. The maximum extent in the box area is more persistent during the 2018–2019 fast-ice cycle. As expected, these variations in fast-ice are similar to those in Lady Newnes Bay. Differences are only observed during maximum fast-ice coverage for the box area during the 2018–2019 fast-ice cycle, while the maximum extension for the whole bay is during the 2019–2020 cycle (Figure 1a).

4.3. PIT Rift Formation Prior to Break-Off

Between 17 February and 1 March 2017, coincident with a period of fast ice break-out, the tip of the ice tongue shifted about 500 m north (Figure 1b). This caused a 2000 m long and up to 150 m wide rift in the southern margin of the grounding zone (Figure 1c). With fast-ice freezing up shortly after the rift opening we did not observe

any further rift activity. This is evidence that the continuous presence of fast ice stabilized the ice tongue and delayed the break-off for another three years. The effect of the fast-ice stabilization can be inferred from the SAR image sequence as the build-up of (multi-year) fast ice makes the rift imperceptible on later image acquisitions. A rift compression might have been caused by the buttressing effect of fast-ice holding its banks in combination with ice flow from the interior reducing the width of the rift. It is also possible that continued snowfall on multi-year fast ice, which filled the rift, made the radar intensity level in the rift similar to the surroundings. Based on our SAR analysis it is almost certain that the break-off in 2020 occurred along the rift which initially formed in 2017 and that the rifting event in 2017 preconditioned the final break-off. Satellite analysis alone does not allow to evaluate the cause-and-effect chain of the rift formation. However, we notice a difference in ice velocity between northern and southern half of the ice tongue in the region of the grounding line, with higher values in the south (Figure 3). It implies higher glaciological stresses in the area of rift opening, which could have been reinforced by changes in fast-ice conditions (Bassis et al., 2008)

4.4. PIT Dynamics Before Break-Off (2017–2020)

We observed seasonal variability of ice tongue surface velocity, with larger mean velocities observed during February, March and April, and lower mean velocities between July and October (Figure 3a). The mean velocity of the ice tongue for the three-year period is 217.9 ± 11.1 m yr^{-1} (Figure 3b), in agreement with other studies (Mouginot et al., 2012; Rignot et al., 2017). During this time the surface mean velocity varies between 194.4 ± 8.3 m yr^{-1} (October 2018) and 242.4 ± 28.7 m yr^{-1} (February 2020). The standard deviations are higher during periods when no fast-ice is present and before the 2020 break-off. This higher variability suggests that the dynamics of the ice tongue not only varies seasonally with fast-ice area change, but also with the presence/absence of fast-ice. There is a statistically significant relationship between fast-ice area and the PIT surface velocity (correlation coefficient of −0.62, R-squared: 0.39 and p-value of 3.77e−11).

After break-off, the ice tongue floated first outwards and was then carried northeast by a coast-parallel current that made it spin counterclockwise (Figure 1d). During the first 12 days the average drift velocity was 1.7 km d^{-1}. The drift stopped soon afterward when the fast-ice started freezing up in April. The ice tongue stayed trapped at the tip of the Icebreaker Ice Tongue during the 2020 fast-ice season about ∼40 km from its original position. In 2021, after the fast-ice receded, it continued its northward drift past Coulman Island and then around Cape Adare following a coastal current to the west.

5. Fast-Ice Variability and Its Implications for Ice Tongue Stability and Dynamics

Our observations support previous studies which show that reduced sea ice extent promotes damaging effects of ice shelves by ocean activity (Massom et al., 2018) or, vice versa, that increased fast ice extent stabilizes marine terminating glaciers (Rott et al., 2018). In a pan-Antarctic context, decreasing sea ice days have been linked with terminus position retreat in Antarctica (Baumhoer et al., 2021; Miles et al., 2016). We found that even relatively short periods of fast-ice break-out can cause calving or serious damage to an ice tongue. Furthermore, we can link variations in ice tongue dynamics to variability in fast-ice extent.

From 1963 until around the year 2005, we focused on the analysis of the length change of the ice tongue and lower resolution information of the fast-ice extent. During this period, the steady growth of the ice tongue was limited by only two major calving events. The first calving happened sometime during the 1980s, the second in 2005. For two dates, PIT exceeded 21 km (3 December 1962 and 19 January 2005) just before major calving events (∼7 km and 3 km, respectively). The higher availability of satellite data after 2005 allowed us to better constrain the periods of continuous growth, to detect smaller calving events, and to observe other signs of change.

5.1. Fast-Ice and Ice Tongue Dynamics

The average velocity of the ice tongue for the 1996–2010 period as depicted in the MEaSUREs data set (208 ± 13m yr^{-1}) (Mouginot et al., 2012) is slightly lower than our mean ice velocity of 217 ± 11m yr^{-1} for the period 2017–2020. However, our velocity measurements are evenly distributed over a 3-year period and potentially more representative, whereas the MEaSUREs velocity data set could be biased towards a particular season of the year. For the observation period 2017–2020, we linked the variability in ice dynamics of PIT to the

seasonal variations of fast-ice coverage. The Sentinel-1 SAR ice velocity time series are relatively short but with a dense temporal resolution (12-day repeat pass over this entire 3 year period), which allowed us to continuously quantify seasonal ice dynamical changes. We found an inverse correlation of −0.62 between the fast-ice cover surrounding the PIT and its surface velocities. The seasonal variability observed is consistent with other studies that show melange and/or fast-ice control on tidewater glacier dynamics and growth (Greene et al., 2018; Krug et al., 2015; Reeh et al., 2001; Zhou et al., 2014). Monthly mean ice surface velocities in March are 11% higher compared to October for the 2017–2020 period.

Similar seasonal fluctuations on ice dynamics of ice shelves have been observed in other parts of Antarctica using more sparse data-sets (Greene et al., 2018; Tomar et al., 2021; Zhou et al., 2014). The reasons for these seasonal changes were partially explained with the advance/retreat of fast-ice, which showed a significant negative correlation with ice velocity fluctuations. Although we are unable to provide insights into the fast-ice thickness evolution for our study area, a previous study showed that modeled sea ice thickness has a good relationship with fluctuations in ice dynamics (Greene et al., 2018). This suggests that not only changes in the fast-ice area, but also the structural integrity or stability of fast-ice, could have impacted the observed ice tongue dynamics. Ice tongue thinning through basal melting could be another cause of seasonal acceleration. This effect is likely smaller than changes in fast-ice/melange over the short period (Krug et al., 2015), and there is no indication that the thickness of floating ice masses in the area have significantly changed (Adusumilli et al., 2020; Paolo et al., 2015).

It has been suggested previously that ice melange buttressing can promote growth by suppressing the calving of glaciers with floating termini (Amundson et al., 2010; Krug et al., 2015; Robel, 2017). Our observations for the 2001 to 2020 interval show a considerable variability in growth rates, ranging from 50 to 271m yr^{-1}. When comparing growth rates with fast-ice coverage we found that faster growth is associated with periods of persistent fast-ice extent and periods of slow growth related to fluctuations in the fast-ice coverage. It indicates an inverse relationship between ice tongue calving and fast-ice extent. Longer periods of extensive fast-ice coverage protect the frontal area of the ice tongue and promote growth in return. These observations support modeling results that found that the presence or absence of fast-ice appears to be a determining factor on the growth of unconfined ice shelves (Wearing et al., 2020).

5.2. PIT 2020 Break-Off

PIT completely detached from the ice in the grounding zone after a period of low fast-ice coverage between 2020. Although calving from ice tongues has been reported before (Massom, 2003), a complete break-off is unseen. Big calving events of ice tongues have been associated with strong storms (Frezzotti & Mabin, 1994), collision with bigger icebergs (MacAyeal et al., 2008; Massom et al., 2015; Young et al., 2010) and sea ice free periods (Aoki, 2017; Miles et al., 2017; Stevens et al., 2013). Major ice tongue calving events in the Western Ross Sea are rare (Frezzotti, 1997). During the last 30 years, major calving events have been reported for the Erebus (Robinson & Haskell, 1990; Stevens et al., 2013) and Drygalski ice tongues (Parmiggiani & Fragiacomo, 2005). The Drygalski calving events from 2005 and 2006 are a result of collisions with B15A and C16, which were giant icebergs originating from the Ross Ice Shelf (MacAyeal et al., 2008; Wuite et al., 2009). In this study, we can directly relate the rifting (February 2017) and break-off (February 2020) of the PIT to the prolonged absence of fast-ice, corroborating similar observations from the Erebus ice tongue (Robinson & Haskell, 1990; Stevens et al., 2013). The absence of fast-ice exposed the ice tongue to oceanic processes, which then affected the ice tongue integrity demonstrating the importance of fast-ice to maintain the structural stability of ice margins.

The precise causes of the break-off are yet to be determined. Considering a prolonged period of fast-ice retreat, offshore winds and local currents (Figure 1d) might have exerted enough pressure to the side of the ice tongue to trigger such an event. Ice tongues represent a floating barrier to surface ocean currents, and the resulting force increasing with the distance to the coast causes internal stress which needs to be balanced by internal forces (Stevens et al., 2017). Legrésy et al. (2004) observed that tidal currents generate lateral pressure on ice tongues, and Stevens et al. (2013) suggested that this kind of mechanism could cause structural failure. The geometry of PIT showed a very high length to width ratio, which certainly represented an effective lever for a lateral force. The observed drift of almost 2 km d^{-1} and simultaneous rotation of the ice tongue immediately after calving suggests that such lateral forces were indeed present (Figure 1d). Ocean swell has also been proposed as a mechanism of failure for ice tongues and ice shelves (Holdsworth & Glynn, 1978; Massom et al., 2018).

The complete calving of an ice tongue just within a few ice thicknesses from its grounding line has not been reported before. Considering the observed growth rates and the present-day fast-ice conditions, the re-advance of the ice tongue to its typical previous length seems rather unlikely. Based on our observations, PIT requires 108.8 ± 24.9 years of growth to reach the near maximum length estimated for 1957/62. A complete earlier break-off over the full length could have therefore only occurred around the mid-19th century. Analysis of diatoms retrieved from marine sediments about 30 km south of PIT suggests extremely persistent fast-ice conditions over the last 900 years (Mezgec et al., 2017) and therefore rather implies an one in a thousand year event at this particular location. Mezgec et al. (2017) found a strong relationship between latent-heat polynya formation, katabatic winds, and the persistence of coastal sea ice. Variability in this sensitive regime could have potentially triggered fast-ice changes and the PIT collapse. It might affect other nearby ice tongues in the future, although different geographic settings and ice tongue geometries will change the response to variations in external forcing.

6. Summary and Conclusions

Through the lens of a unique calving event, we showed that fast-ice is a stabilizing factor delaying ice tongue collapse and that fast-ice affects seasonal ice tongue dynamics. We conclude that the stability provided by continuous (multi-year) fast-ice was critical in delaying the PIT break-off. In the absence of obvious other forcings, we conclude that the PIT break-off, pre-conditioned by a significant rift formation two years earlier, was possibly triggered by local ocean currents, swell or a combination of both. Our findings support evidence that fast-ice can suppress major calving events of floating ice masses.

In addition, we established a clear relationship between the seasonal variation of ice-tongue velocity and fast ice extent. Ice velocities during summer, when less fast ice is present, are up to 11% higher than in winter. We therefore conclude further, in absence of any other obvious causes, that fast ice exerts a significant buttressing force on this particular ice tongue. The analysis of ice dynamics is based on a continuous 3-year long time series of 12-day repeat pass satellite data. Further analysis is required to better understand the interaction between fast-ice and floating glacier ice, how the size and shape of ice tongues alters this relationship, and if a two way relationship in the absence of ice tongues will affect fast-ice building and coverage.

Finally, our observations indicate that fast-ice is an essential component of the ice tongue growth cycle and periods of prolonged fast-ice buttressing allow continuous advance. The unconfined nature of ice tongues and their relatively small size make them a suitable subject to study sea ice buttressing effects on floating ice, because they are potentially more sensitive to fast-ice changes. Future changes in fast-ice coverage, thickness and duration could affect the growth rate and dynamics of Antarctic ice tongues.

Data Availability Statement

We acknowledge the use of imagery from ESA (available through https://search.asf.alaska.edu), NASA (available through https://earthexplorer.usgs.gov/), and USGS (available through https://earthexplorer.usgs.gov/). The surface velocity data created using GammaSAR (https://www.gamma-rs.ch/software), and used in this study is available at https://doi.org/10.5281/zenodo.5725911.

Acknowledgments
R. Gomez-Fell acknowledges the support by the University of Canterbury and the Antarctic New Zealand Sir Robin Irvine Doctoral Scholarships. W. Rack was partially funded by the New Zealand Antarctic Science Platform. The comments of the two reviewers (Craig Stevens and one anonymous) greatly improved the final manuscript.

References

Adusumilli, S., Fricker, H. A., Medley, B., Padman, L., & Siegfried, M. R. (2020). Interannual variations in meltwater input to the Southern Ocean from Antarctic ice shelves. *Nature Geoscience* (Vol. 13, pp. 616–620). https://doi.org/10.1038/s41561-020-0616-z

Amundson, J. M., Fahnestock, M., Truffer, M., Brown, J., Lüthi, M. P., & Motyka, R. J. (2010). Ice mélange dynamics and implications for terminus stability, Jakobshavn Isbrse, Greenland. *Journal of Geophysical Research: Earth Surface*, *115*(1), 1–12. https://doi.org/10.1029/2009JF001405

Aoki, S. (2017). Breakup of land-fast sea ice in Lützow-Holm Bay, East Antarctica, and its teleconnection to tropical Pacific sea surface temperatures. *Geophysical Research Letters*, *44*(7), 3219–3227. https://doi.org/10.1002/2017gl072835

Bassis, J. N., Fricker, H. A., Coleman, R., & Minster, J.-B. (2008). An investigation into the forces that drive ice-shelf rift propagation on the Amery Ice Shelf, East Antarctica. *Journal of Glaciology*, *54*(184), 17–27. https://doi.org/10.3189/002214308784409116

Baumhoer, C. A., Dietz, A. J., Kneisel, C., Paeth, H., & Kuenzer, C. (2021). Environmental drivers of circum-Antarctic glacier and ice shelf front retreat over the last two decades. *The Cryosphere*, *15*(5), 2357–2381. https://doi.org/10.5194/tc-15-2357-2021

Bindschadler, R., Choi, H., Wichlacz, A., Bingham, R., Bohlander, J., Brunt, K., et al. (2011). Getting around Antarctica: New high-resolution mappings of the grounded and freely-floating boundaries of the Antarctic ice sheet created for the International Polar Year. *Cryosphere*, *5*(3), 569–588. https://doi.org/10.5194/tc-5-569-2011

Brett, G. M., Irvin, A., Rack, W., Haas, C., Langhorne, P. J., & Leonard, G. H. (2020). Variability in the distribution of fast ice and the sub-ice platelet layer near McMurdo ice shelf. *Journal of Geophysical Research: Oceans*, *125*(3), 1–21. https://doi.org/10.1029/2019JC015678

Burnett, M. G. (2012). *Hexagon (KH-9)–Mapping camera program and evolution, national reconnaissance office (NRO)*. Center for the Study of National Reconnaissance (CSNR).

Cassotto, R. K., Burton, J. C., Amundson, J. M., Fahnestock, M. A., & Truffer, M. (2021). Granular decoherence precedes ice mélange failure and glacier calving at Jakobshavn Isbræ. *Nature Geoscience* (Vol. 14, pp. 417–422). https://doi.org/10.1038/s41561-021-00754-9

Depoorter, M. A., Bamber, J. L., Griggs, J. A., Lenaerts, J., Ligtenberg, S. R., Van Den Broeke, M. R., & Moholdt, G. (2013). Calving fluxes and basal melt rates of Antarctic ice shelves. *Nature*, *502*(7469), 89–92. https://doi.org/10.1038/nature12567

Fountain, A. G., Glenn, B., & Scambos, T. (2017). The changing extent of the glaciers along the western Ross Sea, Antarctica. *Geology*, *45*(10), 927–930. https://doi.org/10.1130/G39240.1

Fraser, A. D., Massom, R. A., Ohshima, K. I., Willmes, S., Kappes, P. J., Cartwright, J., & Porter-Smith, R. (2020). High-resolution mapping of circum-Antarctic landfast sea ice distribution, 2000–2018. *Earth System Science Data*, *12*(4), 2987–2999. https://doi.org/10.5194/essd-12-2987-2020

Fraser, A. D., Ohshima, K. I., Nihashi, S., Massom, R. A., Tamura, T., Nakata, K., et al. (2019). Landfast ice controls on sea-ice production in the Cape Darnley polynya: A case study. *Remote Sensing of Environment*, *233*(April), 111315. https://doi.org/10.1016/j.rse.2019.111315

Frezzotti, M. (1993). Glaciological study in Terra Nova Bay, Antarctica inferred from remote sensing analysis. *Annals of Glaciology*, *17*, 63–71. https://doi.org/10.1017/s0260305500012623

Frezzotti, M. (1997). Ice front fluctuation, iceberg calving flux and mass balance of Victoria Land glaciers. *Antarctic Science*, *9*(1), 61–73. https://doi.org/10.1017/s0954102097000096

Frezzotti, M., & Mabin, M. (1994). 20th century behaviour of Drygalski ice tongue, Ross Sea, Antarctica. *Annals of Glaciology*, *20*(1993), 397–400. https://doi.org/10.3189/1994aog20-1-397-400

Greene, C. A., Young, D. A., Gwyther, D. E., Galton-Fenzi, B. K., & Blankenship, D. D. (2018). Seasonal dynamics of Totten Ice Shelf controlled by sea ice buttressing. *Cryosphere*, *12*(9), 2869–2882. https://doi.org/10.5194/tc-12-2869-2018

Haas, C., Langhorne, P. J., Rack, W., Leonard, G. H., Brett, G. M., Price, D., et al. (2021). Airborne mapping of the sub-ice platelet layer under fast ice in McMurdo Sound, Antarctica. *The Cryosphere*, *15*(1), 247–264. https://doi.org/10.5194/tc-15-247-2021

Holdsworth, G. (1969). Flexure of a floating ice tongue. *Journal of Glaciology*, *8*(54), 385–397. https://doi.org/10.1017/s0022143000026976

Holdsworth, G. (1982). Dynamics of Erebus Glacier Tongue. *Annals of Glaciology*, *3*, 131–137. https://doi.org/10.1017/s0260305500002652

Holdsworth, G., & Glynn, J. (1978). Iceberg calving from floating glaciers by a vibrating mechanism. *Nature*, *274*(5670), 464–466. https://doi.org/10.1038/274464a0

Howat, I. M., Box, J. E., Ahn, Y., Herrington, A., & McFadden, E. M. (2010). Seasonal variability in the dynamics of marine-terminating outlet glaciers in Greenland. *Journal of Glaciology*, *56*(198), 601–613. https://doi.org/10.3189/002214310793146232

Krug, J., Durand, G., Gagliardini, O., & Weiss, J. (2015). Modelling the impact of submarine frontal melting and ice mélange on glacier dynamics. *Cryosphere*, *9*(3), 989–1003. https://doi.org/10.5194/tc-9-989-2015

Legrésy, B., Wendt, A., Tabacco, I., Rémy, F., & Dietrich, R. (2004). Influence of tides and tidal current on Mertz Glacier, Antarctica. *Journal of Glaciology*, *50*(170), 427–435. https://doi.org/10.3189/172756504781829828

Li, X., Ouyang, L., Hui, F., Cheng, X., Shokr, M., & Heil, P. (2018). An improved automated method to detect landfast ice edge off Zhongshan station using SAR imagery. *IEEE Journal of Selected Topics in Applied Earth Observations and Remote Sensing*, *11*(12), 4737–4746. https://doi.org/10.1109/JSTARS.2018.2882602

MacAyeal, D. R., Okal, M. H., Thom, J. E., Brunt, K. M., Kim, Y. J., & Bliss, A. K. (2008). Tabular iceberg collisions within the coastal regime. *Journal of Glaciology*, *54*(185), 371–386. https://doi.org/10.3189/002214308784886180

Mahoney, A., & Eicken, H. (2004). Landfast sea ice extent and variability in the alaskan arctic derived from SAR imagery. In *IEEE International Geoscience and Remote Sensing Symposium, 2004* (Vol. 3, pp. 2146–2149). IEEE. https://doi.org/10.1109/IGARSS.2004.1370783

Massom, R. A. (2003). Recent iceberg calving events in the Ninnis Glacier region, East Antarctica. *Antarctic Science*, *15*(2), 303–313. https://doi.org/10.1017/S0954102003001299

Massom, R. A., Giles, A. B., Fricker, H. A., Warner, R. C., Legrésy, B., Hyland, G., et al. (2010). Examining the interaction between multi-year landfast sea ice and the Mertz Glacier Tongue, East Antarctica: Another factor in ice sheet stability? *Journal of Geophysical Research: Oceans*, *115*(12), 1–15. https://doi.org/10.1029/2009JC006083

Massom, R. A., Giles, A. B., Warner, R. C., Fricker, H. A., Legrésy, B., Hyland, G., et al. (2015). External influences on the Mertz Glacier Tongue (East Antarctica) in the decade leading up to its calving in 2010. *Journal of Geophysical Research: Earth Surface*, *120*(3), 490–506. https://doi.org/10.1002/2014JF003223

Massom, R. A., Scambos, T., Bennetts, L. G., Reid, P., Squire, V., & Stammerjohn, S. E. (2018). Antarctic ice shelf disintegration triggered by sea ice loss and ocean swell. *Nature*, *558*(7710), 383–389. https://doi.org/10.1038/s41586-018-0212-1

Mezgec, K., Stenni, B., Crosta, X., Masson-Delmotte, V., Baroni, C., Braida, M., et al. (2017). Holocene sea ice variability driven by wind and polynya efficiency in the Ross Sea. *Nature Communications*, *8*(1), 1334. https://doi.org/10.1038/s41467-017-01455-x

Miles, B. W., Stokes, C. R., & Jamieson, S. S. (2016). Pan–Ice-sheet glacier terminus change of Wilkes Land to sea-ice changes. *Science Advances*, *44*(May), 0–8.

Miles, B. W., Stokes, C. R., & Jamieson, S. S. (2017). Simultaneous disintegration of outlet glaciers in Porpoise Bay (Wilkes Land), East Antarctica, driven by sea ice break-up. *Cryosphere*, *11*(1), 427–442. https://doi.org/10.5194/tc-11-427-2017

Miles, B. W., Stokes, C. R., Vieli, A., & Cox, N. J. (2013). Rapid, climate-driven changes in outlet glaciers on the Pacific coast of East Antarctica. *Nature*, *500*(7464), 563–566. https://doi.org/10.1038/nature12382

Moon, T., Joughin, I., & Smith, B. (2015). Seasonal to multiyear variability of glacier surface velocity, terminus position, and sea ice/ice mélange in northwest Greenland. *Journal of Geophysical Research: Earth Surface*, *120*(5), 818–833. https://doi.org/10.1002/2015JF003494

Mouginot, J., Scheuchl, B., & Rignot, E. (2012). Mapping of ice motion in Antarctica using synthetic-aperture radar data. *Remote Sensing*, *4*(9), 2753–2767. https://doi.org/10.3390/rs4092753

Nihashi, S., & Ohshima, K. I. (2015). Circumpolar mapping of Antarctic coastal polynyas and landfast sea ice: Relationship and variability. *Journal of Climate*, *28*(9), 3650–3670. https://doi.org/10.1175/JCLI-D-14-00369.1

Padman, L., Siegfried, M. R., & Fricker, H. A. (2018). Ocean tide influences on the Antarctic and Greenland ice sheets. *Reviews of Geophysics*, *56*(1), 142–184. https://doi.org/10.1002/2016RG000546

Paolo, F. S., Fricker, H. A., & Padman, L. (2015). Volume loss from Antarctic ice shelves is accelerating. *Science*, *348*(6232), 327–331. https://doi.org/10.1126/science.aaa0940

Parmiggiani, F., & Fragiacomo, C. (2005). The calving event of the Drygalski ice tongue of February 2005. *International Journal of Remote Sensing*, *26*(21), 4633–4638. https://doi.org/10.1080/01431160500238828

Pritchard, H., Ligtenberg, S., Fricker, H., Vaughan, D., van den Broeke, M., & Padman, L. (2012). Antarctic ice-sheet loss driven by basal melting of ice shelves. *Nature*, *484*(7395), 502–505. https://doi.org/10.1038/nature10968

Rack, W., & Rott, H. (2004). Pattern of retreat and disintegration of the Larsen B ice shelf, Antarctic Peninsula. *Annals of Glaciology*, *39*, 505–510. https://doi.org/10.3189/172756404781814005

Reeh, N., Thomsen, H. H., Higgins, A. K., & Weidick, A. (2001). Sea ice and the stability of north and northeast Greenland floating glaciers. *Annals of Glaciology*, *33*, 474–480. https://doi.org/10.3189/172756401781818554

Rignot, E., Mouginot, J., & Scheuchl, B. (2017). *MEaSUREs InSAR-based Antarctica ice velocity map*. NASA National Snow and Ice Data Center Distributed Active Archive Center. https://doi.org/10.5067/D7GK8F5J8M8R

Rignot, E., Mouginot, J., Scheuchl, B., van den Broeke, M., van Wessem, M. J., & Morlighem, M. (2019). Four decades of Antarctic ice sheet mass balance from 1979–2017. *Proceedings of the National Academy of Sciences*, *116*(4), 1095–1103. https://doi.org/10.1073/pnas.1812883116

Robel, A. A. (2017). Thinning sea ice weakens buttressing force of iceberg mélange and promotes calving. *Nature Communications*, *8*(1), 14596. https://doi.org/10.1038/ncomms14596

Robinson, W., & Haskell, T. (1990). Calving of Erebus glacier tongue. *Nature*, *346*, 615–616. https://doi.org/10.1038/346615b0

Rott, H., Abdel Jaber, W., Wuite, J., Scheiblauer, S., Floricioiu, D., van Wessem, J. M., et al. (2018). Changing pattern of ice flow and mass balance for glaciers discharging into the Larsen A and B embayments, Antarctic Peninsula, 2011 to 2016. *The Cryosphere*, *12*(4), 1273–1291. https://doi.org/10.5194/tc-12-1273-2018

Stevens, C., McPhee, M. G., Forrest, A. L., Leonard, G. H., Stanton, T., & Haskell, T. (2014). The influence of an Antarctic glacier tongue on near-field ocean circulation and mixing. *Journal of Geophysical Research: Oceans*, *119*(4), 2344–2362. https://doi.org/10.1002/2013JC009070

Stevens, C., Sang Lee, W., Fusco, G., Yun, S., Grant, B., Robinson, N., & Yeon Hwang, C. (2017). The influence of the Drygalski Ice Tongue on the local ocean. *Annals of Glaciology*, *58*(74), 51–59. https://doi.org/10.1017/aog.2017.4

Stevens, C., Sirguey, P., Leonard, G. H., & Haskell, T. (2013). Brief communication: "The 2013 Erebus glacier tongue calving event". *Cryosphere*, *7*(5), 1333–1337. https://doi.org/10.5194/tc-7-1333-2013

Strozzi, T., Luckman, A., Murray, T., Wegmuller, U., & Werner, C. L. (2002). Glacier motion estimation using SAR offset-tracking procedures. *IEEE Transactions on Geoscience and Remote Sensing*, *40*(11), 2384–2391. https://doi.org/10.1109/TGRS.2002.805079

Todd, J., & Christoffersen, P. (2014). Are seasonal calving dynamics forced by buttressing from ice mélange or undercutting by melting? Outcomes from full-Stokes simulations of store glacier, West Greenland. The *Cryosphere*, *8*(6), 2353–2365. https://doi.org/10.5194/tc-8-2353-2014

Todd, J., Christoffersen, P., Zwinger, T., Räback, P., & Benn, D. I. (2019). Sensitivity of a calving glacier to ice-ocean interactions under climate change: New insights from a 3-d full-Stokes model. *Cryosphere*, *13*(6), 1681–1694. https://doi.org/10.5194/tc-13-1681-2019

Tomar, K. S., Kumari, S., & Luis, A. J. (2021). Seasonal ice flow velocity variations of polar record glacier, East Antarctica during 2016-2019 using sentinel-1 data. *Geocarto International*, *0*(0), 1–12. https://doi.org/10.1080/10106049.2021.1892211

Truffer, M., & Motyka, R. J. (2016). Where glaciers meet water: Subaqueous melt and its relevance to glaciers in various settings. *Reviews of Geophysics*, *54*(1), 220–239. https://doi.org/10.1002/2015RG000494

Vijay, S., & Braun, M. (2017). Seasonal and interannual variability of Columbia glacier, Alaska (2011-2016): Ice velocity, mass flux, surface elevation and front position. *Remote Sensing*, *9*(6), 1–18. https://doi.org/10.3390/rs9060635

Wearing, M. G., Kingslake, J., & Worster, M. G. (2020). Can unconfined ice shelves provide buttressing via hoop stresses? *Journal of Glaciology*, *66*(257), 349–361. https://doi.org/10.1017/jog.2019.101

Wegmüller, U., Werner, C., Strozzi, T., Wiesmann, A., Frey, O., & Santoro, M. (2016). Sentinel-1 support in the GAMMA software. *Procedia Computer Science*, *100*, 1305–1312. https://doi.org/10.1016/j.procs.2016.09.246https://linkinghub

Wuite, J., Jezek, K. C., Wu, X., Farness, K., & Carande, R. (2009). The velocity field and flow regime of David glacier and Drygalski ice tongue, Antarctica. *Polar Geography*, *32*(3–4), 111–127. https://doi.org/10.1080/10889370902815499

Young, N. W., Legresy, B., Coleman, R., & Massom, R. (2010). *Mertz Glacier tongue unhinged by giant iceberg*. Australian Antarctic Magazine(18), 2010. Retrieved from http://search.informit.com.au/documentSummary;dn=455688926704560;res=ielhss

Zhou, C., Zhou, Y., Deng, F., Ai, S., Wang, Z., & Dongchen, E. (2014). Seasonal and interannual ice velocity changes of polar record glacier, east Antarctica. *Annals of Glaciology*, *55*(66), 45–51. https://doi.org/10.3189/2014AoG66A185

References From the Supporting Information

Howat, I. M., Porter, C., Smith, B. E., Noh, M. J., & Morin, P. (2019). The reference elevation model of Antarctica. The *Cryosphere*, *13*(2), 665–674. https://doi.org/10.5194/tc-13-665-2019

Lemos, A., Shepherd, A., McMillan, M., Hogg, A. E., Hatton, E., & Joughin, I. (2018). Ice velocity of Jakobshavn Isbræ, Petermann glacier, Nioghalvfjerdsfjorden, and Zachariæ Isstrøm, 2015–2017, from sentinel 1-a/b SAR imagery. *The Cryosphere*, *12*(6), 2087–2097. https://doi.org/10.5194/tc-12-2087-2018

Mouginot, J., Rignot, E., Scheuchl, B., & Millan, R. (2017). Comprehensive annual ice sheet velocity mapping using Landsat-8, Sentinel-1, and RADARSAT-2 data. *Remote Sensing*, *9*(4), 1–20. https://doi.org/10.3390/rs9040364